ULTRA-COMPACT SMITH-PURCELL FREE-ELECTRON LASER

J. D. Jarvis, J. L. Davidson, B. L. Ivanov, J. L. Kohler, C. A. Brau, Vanderbilt University, Nashville, TN, USA, H. L. Andrews, Los Alamos National Laboratory, Los Alamos, NM, USA

Abstract

There is currently a need for a compact source of coherent THz radiation. In this paper we describe an electrostatically-focused Smith-Purcell free-electron laser that will literally fit in a shirt pocket. It is shown that operation of such a device requires a high-brightness electron beam. In the proposed shirt-pocket SPFEL this is provided by a diamond field-emitter array. A device designed to produce coherent harmonic radiation at 0.22 THz has been constructed and is now being commissioned.

INTRODUCTION

The THz region of the spectrum remains underserved by available sources of coherent radiation [1, 2]. Solid-state sources are feeble, and some require cryogenic operation. High-power, accelerator-based sources are large and expensive [3, 4, 5]. Backward-wave oscillators (BWOs) are commercially available at the low end of the THz range and can be frequency-multiplied to higher frequencies at microwatt power levels [6]. However, magnetic focusing makes them heavy and cumbersome.

In this paper we describe an electrostatically-focused Smith-Purcell free-electron laser (SPFEL). Fundamentally, an SPFEL is similar to a BWO, and an absolute instability causes an evanescent wave of the grating to be excited by the electron beam. This wave bunches the electrons at the frequency of the wave, and in an SPFEL coherent harmonics of the BWO mode are emitted as Smith-Purcell radiation [7]. Electrostatic focusing is possible because the electron source is a high-brightness diamond field-emitter array, which operates conveniently at room temperature [8]. This reduces the size and complexity of the device to the point where it might literally fit into a shirt pocket.

DESCRIPTION OF THE DEVICE

A schematic diagram of the Shirt-Pocket SPFEL is shown in Fig. 1. The electron beam is emitted from a diamond field-emitter array cathode at potential $V_0 = 0$,

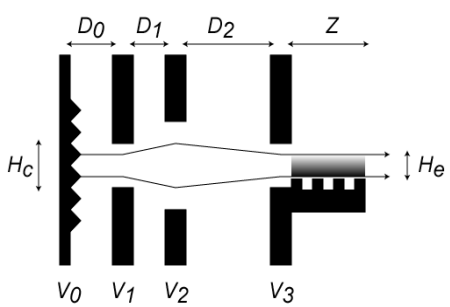

Figure 1: Schematic diagram of a Shirt-Pocket FEL.

Table I: Parameters of the Shirt-Pocket SPFEL.

$Z = 30$ mm	Grating length
$W = 6$ mm	Grating width
$L = 200$ microns	Grating period
$A = 200$ microns	Groove width
$H = 575$ microns	Groove depth
$V = 20$ keV	Electron energy
$W(cathode) = 5$ mm	Beam width

accelerated to the anode at potential V_1, focused by the second electrode at potential V_2, further accelerated to the grating at potential V_3, passes over the grating, and exits the device. Some typical parameters are summarized in Table I.

To compute the performance of the SPFEL, including the effects of side walls on the grating, we use the 3-D theory developed previously [9]. The dispersion of the grating is shown in Fig. 2. The operating point is the intersection of the dispersion curve with the light line. Since the electron beam uniformly fills most of the region between the walls, we assume that only the fundamental transverse mode is excited. We ignore the effects of reflections at the ends of the grating. At high frequencies, the THz fields generate surface currents in the grating, and dissipative losses associated with these currents attenuate the evanescent wave. In computing the dissipative losses in the surfaces of the grating, we ignore losses in the sidewalls. Typically, the width of the grating is two orders of magnitude larger than the scale height of the evanescent wave, so the sidewalls contribute very little. Since the grating is wide, we assume that the attenuation rate for waves travelling along the grating is the same as that for waves in a grating without sidewalls,

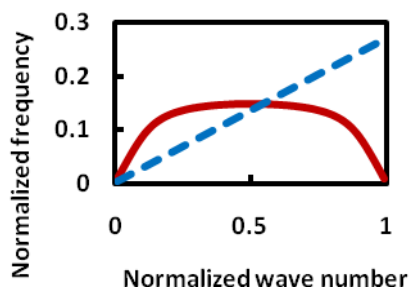

Figure 2: Dispersion relation for the shirt-pocket FEL. Red curve: normalized frequency versus normalized wave number; blue curve: beam line.

which has been calculated previously [10]. The principal effect of the sidewalls is to change the group velocity of the evanescent wave. Since the device operates close to the Bragg point, where the group velocity vanishes, the group velocity is very sensitive to the details of the dispersion relation. The group velocity is important because it must be negative to sustain an absolute instability, but small since the gain increases inversely as the cube root of the group velocity. However, the attenuation due to losses in the grating increases inversely as the group velocity [10]. Thus, losses dominate when the synchronous point is too close to the Bragg point.

To compute the gain, it is necessary to know the current density and filling factor of the electron beam over the grating. To do this we assume that the beam uniformly overfills the region of the evanescent wave. We further assume that the angular distribution of the electron trajectories is large, and select from this distribution only electrons from that region of the vertical (x-direction) phase space for which the angle of the trajectory is sufficiently small that the vertical displacement from one end of the grating to the other is less than the scale height of the evanescent wave. Thus, in the paraxial approximation, we consider only electrons for which

$$\frac{|p_x|}{p} < \frac{h_e}{Z}$$

where p_x is the vertical momentum, p the total momentum, Z the length of the grating, and $h_e = \beta\gamma\lambda_\infty / 4\pi$ the scale height of the evanescent wave, in which λ_∞ is the wavelength of the evanescent wave in free space and β, γ are the relativistic parameters of the electrons. For the horizontal (y) direction we assume that the transverse momentum can be ignored. This is true if the transverse momentum (p_y) doesn't slow the electrons in the longitudinal direction enough to de-phase them relative to the evanescent wave. For a given kinetic energy (ignoring the vertical momentum), the change in the longitudinal velocity is $|\Delta v / v| \approx p_y^2 / 2p^2$, so the phase error accumulated traversing the length of the grating is $k|\Delta z| \approx kLp_y^2 / 2p^2$, where k is the wave number of the evanescent wave. For waves near the Bragg point ($k \approx K/2$, where K is the wave number of the grating), the restriction $k|\Delta z| < 1$ is equivalent to the requirement

$$\frac{|p_y|}{p} < \frac{1}{\sqrt{N_g}}$$

where N_g the number of periods along the grating. For typical grating parameters, the condition on p_y is less restrictive than the condition on p_x and can be ignored.

To compute the useful current density over the grating we take advantage of Liouville's theorem, which states that the density in phase space is constant along a trajectory. Emittance growth caused by nonlinear forces occurs by phase-space dilution, but this is most important near the edges of the region of phase space occupied by the beam. As we shall see, the useful region of phase space is near the center of the occupied region. The phase-space current density at the cathode is $J_\phi = J_{cathode} / \Delta p_{cathode}$, where $J_{cathode}$ is the current density at the cathode and $\Delta p_{cathode}$ is the momentum spread at the cathode. But for a uniformly emitting cathode of width $\Delta x_{cathode}$, the rms normalized emittance is

$$\varepsilon_N = \frac{1}{mc}\sqrt{\langle x^2 \rangle \langle p^2 \rangle} = \frac{\Delta x_{cathode} \Delta p_{cathode}}{12mc}$$

From measurements we have made, we find that $\Delta p_{cathode} / mc = 1.2 \times 10^{-2}$ [11]. The useful current density over the grating is then

$$\frac{J}{J_{cathode}} = \frac{2h_e}{Z}\frac{\beta\gamma mc}{\Delta p_{cathode}}$$

Although the beam is assumed to overfill the region above the grating, the filling factor is less than unity. Near the grating the current is reduced because the grating intercepts electrons that arrive from below the grating and electrons that strike the grating from above. If we place ourselves at the middle of the grating, we see that at the grating surface the number of electrons that don't pass through the grating surface vanishes, but the number increases linearly with height until at $x = h_e/2$ all electrons that satisfy the selection criterion miss the grating. The filling factor is therefore [10]

$$F_{fill} = \frac{\int_0^{h_e/2} e^{-x/h_e}\frac{2x}{h_e}dx + \int_{h_e/2}^{\infty} e^{-x/h_e}dx}{\int_0^{\infty} e^{-x/h_e}dx} = 2 - \frac{2}{\sqrt{e}}$$

The parameters of the grating, summarized in Table I, were chosen to place the coherent Smith-Purcell radiation (the second harmonic of the evanescent wave) in the THz region at a frequency of 0.22 THz. At this frequency,

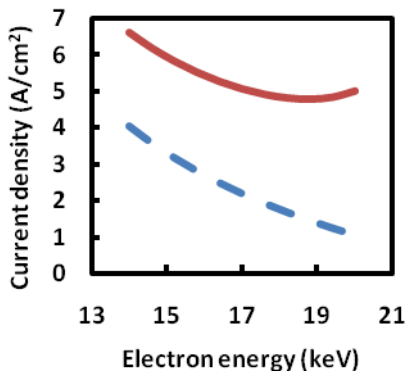

Figure 3 Start current density at the cathode as a function of the electron energy. Solid red curve: grating losses included; dotted blue curve: losses ignored.

Table II Parameters of the Electron Optical System.

$D_0 = 0.5$ mm	Cathode-anode distance
$D_1 = 1$ mm	Anode-focus electrode distance
$D_2 = 7$ mm	Focus electrode grating distance
$T = 0.5$ mm	Electrode thickness
$V_1 = 10$ kV	Anode voltage
$V_2 = 2.5$ kV	Focus electrode voltage
$V_3 = 20$ kV	Grating voltage

and at higher frequencies, losses in the grating surface are very important. For this reason, copper is chosen as the grating material.

The results of the computations are shown in Fig. 3, where the start current density at the cathode is shown as a function of the electron energy. The red curve shows the start current density without losses, the blue curve shows the result when losses are included. Losses increase the start current more than a factor of two. Losses increase sharply at the highest electron energy because the synchronous point approaches the Bragg point, where the group velocity vanishes. The start current density is less than 5 A/cm^2 at 19 kV, which is well within the capability of diamond field-emitter arrays [11]. With an aluminum grating the start current density increases to 7.5 A/cm^2 at 17 kV.

Since the beam overfills the region above the grating, the phase space filled by the beam from the cathode is much larger than that sampled by the grating. To show this, a simple Mathcad code has been written to transform the phase space from the cathode to the center of the grating using the paraxial approximation. The electron optical system is divided into apertures (lenses) and drift spaces, each of which is individually described by a matrix in the usual way [12]. When a drift space includes a uniform accelerating field, the effective length is

$$d = L\frac{\operatorname{arccosh}(\gamma_2) - \operatorname{arccosh}(\gamma_1)}{\gamma_2 - \gamma_1}$$

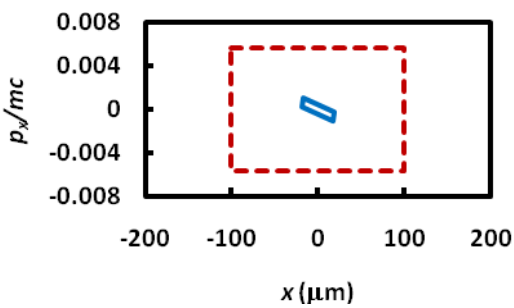

Figure 4 Phase area of the electron beam at the cathode. The useful phase area is enclosed by the blue line.

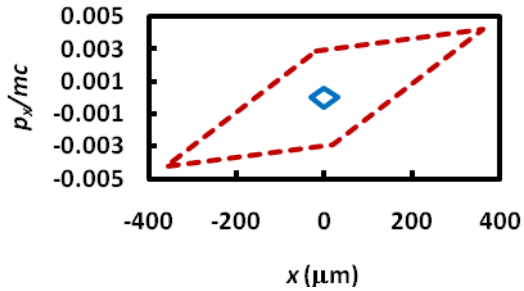

Figure 5 Phase area of the electron beam at the center of the grating. The useful phase area is enclosed by the blue diamond.

in which L is the physical drift length and $\gamma_{1,2}$ are the initial and final relativistic parameters of the electron. The matrices may be multiplied to obtain the overall effect of the optical system, or inverted to transform the phase space backward through the optical system.

The parameters of the electron optical system are summarized in Table II. Some results are shown in Figs. 4 and 5, which show the phase space at the cathode and at the center of the grating. In both cases the useful phase space is a small fraction of the beam phase space. The useful phase space comprises those electrons that remain within the scale height of the evanescent wave through the length of the grating. At the middle of the grating these electrons occupy a diamond-shaped region of phase space whose width is h_e, and whose height is ph_e/Z. The useful phase area (blue solid lines) is much smaller than the total beam phase area (red dotted lines). For the parameters used, the useful phase area is 1.5% of the original phase area. The benefit of this is that if the grating (or the optical column) is misaligned, or the focus voltage is changed, the beam phase area will be distorted and shifted, but for small errors the useable area will remain within the beam area. Thus, the optical system is insensitive to the alignment and focus.

On the other hand, the beam hitting the apertures and the grating will heat and damage the surfaces, so the system can be operated only in microsecond pulses. This

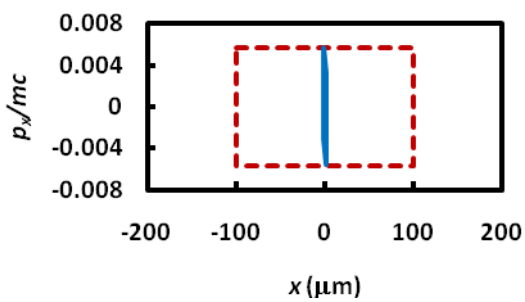

Figure 6 Phase area of the electron beam at the cathode for a focus voltage of 3.23 kV. The useful phase area is enclosed by the blue line.

can be avoided if the cathode size is reduced to the minimum needed to cover the useful phase area. To do this, it is necessary to change the focus voltage so that the useful phase space forms an upright figure at the cathode. Using a focus voltage of 3.23 kV, we get the phase diagram shown in Fig. 6. In this case, the cathode height can be reduced to less than 4 μm and still cover the useful area of phase space. However, the requirements on the focus and alignment are very demanding.

CONCLUSIONS

An electrostatically focused SPFEL shows promise as a compact ("shirt-pocket") source of coherent THz radiation. An SPFEL operates like a BWO, but harmonics of the BWO frequency are emitted as coherent SP radiation. Although operation of a BWO at 1 THz is made difficult by dissipative losses in the grating surface, harmonics of the BWO frequency can be usefully generated across the THz spectrum. Computations made using the theory of coherent harmonics [7] indicate that second-harmonic radiation will be on the order of hundreds of microwatts. This is two orders of magnitude higher than currently available.

Since the phase space of the electron beam is preserved from the cathode to the grating, electrostatic focusing demands a very bright electron beam, which is provided by a DFEA cathode. Computations show the start current density for a small device is on the order of 5 A/cm^2. DFEA cathodes have demonstrated current density as high as 30 A/cm^2, and higher current density may be possible.

Up to the present time, the device has been assembled and is now being commissioned. Preliminary experiments show that the focusing of the electron beam by the optical system agrees with theoretical predictions.

REFERENCES

[1] S. P. Mickan and X.-C. Zhang, Int. J. High-Speed Electron. and Sys. **13**, 601 (2003).

[2] P.H. Siegel, IEEE Trans. Microwave Theory and Techniques, **52**, 2438 (2004).

[3] G. P. Williams, Rev. Sci. Instrum. **73**, 1461 (2002).

[4] G. Ramian, Nucl. Instrum. Methods Phys. Res., Sect. A **318**, 225 (1992).

[5] N. A. Vinokurov, V. P. Bolotin, D. A. Kayran, B. A. Knyazev, E. I. Kolobanov, V.V. Kotenkov, V. V. Kubarev, G. N. Kulipanov, A. N. Matveenko, L. E. Medvedev, S. V. Miginsky, L. A. Mironenko, A. D. Oreshkov, V. K. Ovchar, V. M. Popik, T. V. Salikova, M. A. Scheglov, S. S. Serednyakov, O. A. Shevchenko, and A. N. Skrinsky, "Status of the Novosibirsk Terahertz FEL," presented at the International FEL Conference, Trieste, 30 August-3 September, 2004 (paper TUCOS01, available online in PDF format at http://fel2004.elettra.trieste.it/pls/fel2004/Proceedings.html).

[6] MicroTech Instruments, http://www.mtinstruments.com/thzsources/index.htm.

[7] H. L. Andrews, C. H. Boulware, C. A. Brau, and J. D. Jarvis, Phys. Rev. ST-AB 8, 110702 (2005).

[8] J. D. Jarvis, H.L. Andrews, C. A. Brau, B. K. Choi, J. L. Davidson, W.-P. Kang, Y.-M. Wong, J. Vac. Sci. Tech. B 27, 2264 (2009).

[9] H. L. Andrews, J. D. Jarvis, and C. A. Brau, J. Appl. Phys. 105, 024904 (2009).

[10] H. L. Andrews, C. H Boulware, C. A. Brau, J. T. Donohue, J. Gardelle, J. D. Jarvis, New J. Phys. 8, 289 (2006).

[11] J. D. Jarvis, H. L. Andrews, C. A. Brau, B. K. Choi, J. L. Davidson, Ivanov, W.-P. Kang, C. L. Stewart, and Y.-M. Wong, "Pulsed Uniformity Conditioning and Emittance Measurements of Diamond Field-Emitter Arrays," Proceedings of the 31st International Free Electron Laser Conference, Liverpool, United Kingdom, August 23- 28, 2009.

[12] S. Humphries, Charged Particle Beams (Wiley, New York, 1990), Chapter 4.